



A novel FeNi-based bulk metallic glass with high notch toughness over 70 MPa m^{1/2} combined with excellent soft magnetic properties

Jing Zhou^a, Qianqian Wang^a, Xidong Hui^b, Qiaoshi Zeng^a, Yuwei Xiong^c, Kuibo Yin^c, Baoan Sun^d, Litao Sun^c, Mihai Stoica^e, Weihua Wang^d, Baolong Shen^{a,f,*}

^a School of Materials Science and Engineering, Jiangsu Key Laboratory for Advanced Metallic Materials, Southeast University, Nanjing 211189, China

^b State Key Laboratory for Advanced Metals and Materials, University of Science and Technology Beijing, Beijing 100083, China

^c SEU-FEI Nano-Pico Center, Key Laboratory of MEMS of Ministry of Education, Southeast University, Nanjing 210096, China

^d Institutes of Physics, Chinese Academy of Sciences, Beijing 100190, China

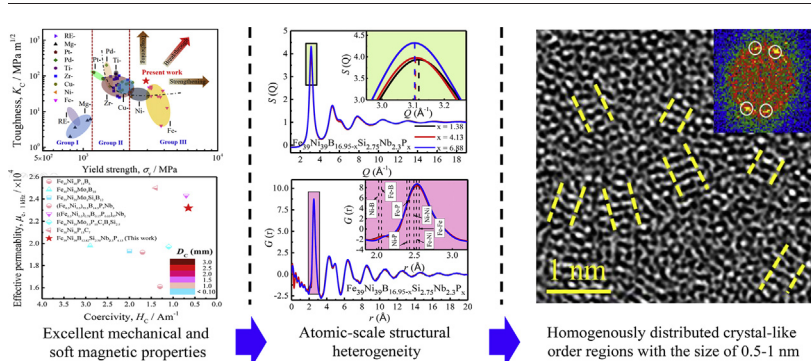
^e Laboratory of Metal Physics and Technology, Department of Materials, ETH, Zurich, 8093 Zurich, Switzerland

^f Institute of Massive Amorphous Metal Science, China University of Mining and Technology, Xuzhou 221116, China

HIGHLIGHTS

- FeNiSiNbP bulk metallic glass with high notch toughness and strength was developed.
- This FeNi-based metallic glass exhibits excellent soft magnetic properties as well.
- Large free volume and high structural disorder degree lead to the high toughness.

GRAPHICAL ABSTRACT



ARTICLE INFO

Article history:

Received 13 October 2019

Received in revised form 20 February 2020

Accepted 21 February 2020

Available online 22 February 2020

Keywords:

FeNi-based BMGs

Notch toughness

Free volume

Structural disorder degree

ABSTRACT

A novel Fe₃₉Ni₃₉B_{12.82}Si_{2.75}Nb_{2.3}P_{4.13} bulk metallic glass (BMG) with high notch toughness of 72.3 MPa m^{1/2}, large plastic strain of 9.8%, high yield strength of 2930 MPa, and a large critical diameter of 2.5 mm was successfully developed. This BMG also exhibits excellent soft magnetic properties, i.e., higher saturation magnetic flux density of 0.86 T, extremely low coercivity of 0.65 A/m, and high effective permeability of 23,250 with high frequency stability. Its toughness value is the highest among Fe-based BMG family. The origin of high toughness was also investigated in detail by using synchrotron X-ray diffraction and aberration-corrected high-resolution transmission electron microscopy. It was found that the high toughness are attributed to atomic-scale structural heterogeneity that resulted from large free volume, high content of metal-metal bonds and high structural disorder degree, which can promote the multiple shear bands and hinder the subsequently propagation. This work provides useful guidelines for developing tough FeNi-based BMGs with high strength and excellent soft magnetic properties from an atomic structural perspective.

© 2020 The Authors. Published by Elsevier Ltd. This is an open access article under the CC BY-NC-ND license (<http://creativecommons.org/licenses/by-nc-nd/4.0/>).

* Corresponding author at: School of Materials Science and Engineering, Jiangsu Key Laboratory for Advanced Metallic Materials, Southeast University, Nanjing 211189, China. E-mail address: blshen@seu.edu.cn (B. Shen).

1. Introduction

Bulk metallic glasses (BMGs) have been attracted great attentions as potential structural materials due to their superhigh strength, high hardness, good wear resistance, and good corrosion resistance [1]. Unlike conventional brittle glasses, metallic glasses are generally capable of limited plastic yielding by shear-band sliding in the presence of a flaw, and thus exhibit toughness-strength relationships that lie between those of ceramics and tough metals [2]. Among them, some Pt-, Zr-, Ti-, and Pd-based BMGs or BMG matrix composites exhibit high fracture toughness, due to an unusual capacity for shielding an opening crack by the extensive shear-band sliding process [2–9]. For example, Pt_{57.5}Cu_{14.7}Ni_{5.3}P_{22.5} BMG [3] exhibits fracture toughness of 80 MPa m^{1/2}, and Zr_{39.6}Ti_{33.9}Nb_{7.6}Cu_{6.4}Be_{12.5} BMG composite [4] dispersed with a soft dendritic phase shows fracture toughness of 173 MPa m^{1/2}. Besides, a monolithic Pd_{82.5}P₆Si_{9.5}Ge₂ BMG with fracture toughness as high as 200 MPa m^{1/2} was developed, and its toughness is the highest value among all BMG systems [2]. However, those tough BMGs or BMG composites usually contain toxic (e.g. Be) or extremely expensive (e.g. Pd and Pt) elements that limit their applications. Therefore, it is necessary to search for tough BMGs with non-toxic and low-cost elements.

Fe-based BMGs are more attractive for applications as structural and functional materials, because of their superhigh strength and excellent soft magnetic properties as well as low costs and good availability of iron [10–13]. However, the poor plasticity and low fracture toughness of most Fe-based BMGs severely hinder their applications. Fortunately, great efforts have been devoted to improve the plasticity of Fe-based BMGs [14–17], e.g., the plastic Fe₅₀Ni₃₀P₁₃C₇ BMG with large plastic strain up to 50% was successfully developed [17,18]. On the other hand, the fracture toughness of Fe-based BMG was also improved from 3 to 52 MPa m^{1/2} by Poon and Johnson et al. through compositional design [19–22]. Besides, introducing secondary phase in Fe-based BMG was also tried. As a result, the Fe₇₇Mo₅P₉C_{7.5}B_{1.5} BMG composite [23] dispersed with α -Fe dendrite phase was prepared by modifying the composition of Fe_{74.5}Mo_{5.5}P_{12.5}C₅B_{2.5} BMG [22]. Nevertheless, the toughness decreased from 52 to 40 MPa m^{1/2}. In addition, the magnetic domains will be pinned by secondary phase, leading to deterioration of soft magnetic properties. Therefore, the method of introducing the secondary phase to glass matrix is not suitable for ferromagnetic BMGs needing to keep their soft magnetic properties. Recent studies showed that the nanoscale heterogeneous structures in BMGs can hinder the propagation of shear bands and increase the number of possible nucleation sites for new shear bands, and thus induce a more uniform deformation with high-density shear band branching and interactions [24]. Interestingly, the increased toughness of Fe-based BMGs mentioned above [20–22] is attributed to the lower activation barriers for shear flow caused by the formation of a “backbone” liquid structure [22], which can be further associated with the heterogeneity in atomic structure [18]. Hence, tailoring inhomogeneity of BMGs in atomic-scale is considerable to improve the fracture toughness for ferromagnetic BMGs while keeping their good soft magnetic properties.

In this study, we focused on FeNi-based metallic glasses, because the FeNi-based metallic glasses exhibit high permeability and have been used to partly substitute the permalloys in sensors, switching transformers and anti-theft labels [25]. In addition, the FeNi-based BMGs can be fabricate into magnetic electronic microparts with high dimensional accuracy in complex geometries, which further extension their potential application as structural and functional materials. Nevertheless, as the same of the other Fe-based BMGs, its fracture toughness is low. For example, the fracture toughness of FeNiVSiB glassy alloy is only 8 MPa m^{1/2}, which is even worse than conventional silicate glasses [26]. The extremely low toughness of FeNi-based BMGs not only makes the manufacturing processes difficult, but also reduces the reliability and safety during service. Therefore, preparation of tough FeNi-based BMGs with excellent soft magnetic properties would be desired.

However, the progress in the aspect is limited. There are few data available to date on the toughness of FeNi-based BMGs, let alone the optimization of alloys for toughness.

As mentioned formerly that the plasticity and toughness of FeNi-based BMG would be improved through increasing the atomic structural heterogeneity by modifying the composition. Based on this consideration, an alloy system from FeNiBSiNbP [27,28] with adjusting the P/B atomic ratio was developed to increase the structural heterogeneity, since the mixing enthalpy of B—P atomic pair is +0.5 kJ/mol [29]. As a result, a novel Fe₃₉Ni₃₉B_{12.82}Si_{2.75}Nb_{2.3}P_{4.13} BMG with diameter up to 2.5 mm was prepared. This FeNi-based BMG exhibited excellent mechanical properties, i.e., high notch toughness (K_Q) of 72.3 MPa m^{1/2}, large plasticity (ϵ_p) of 9.8%, high yield strength (σ_y) of 2930 MPa, as well as excellent soft magnetic properties i.e., higher saturation magnetic flux density (B_s) of 0.86 T, extremely low coercivity (H_c) of 0.65 A/m, and high effective permeability (μ_e) of 23,250. Furthermore, the structural evolution of FeNi-based BMGs varying with the compositions was also investigated in detail. The atomic-scale structure of the samples was investigated by synchrotron X-ray diffraction (XRD) and high-resolution transmission electron microscopy (HRTEM). Based on the theory of structural heterogeneity, underlying mechanism for superhigh toughness are discussed. This work is believed to have the implication for developing new ductile FeNi-based BMGs combined with excellent magnetic properties.

2. Methods

Master alloy ingots with nominal compositions of Fe₃₉Ni₃₉B_{16.95}-xSi_{2.75}Nb_{2.3}P_x (x = 1.38, 2.75, 4.13, 5.5, 6.88 and 8.25 at.%, denoted further as 1.38 at.%, 2.75 at.%, 4.13 at.%, 5.5 at.%, 6.88 at.%, and 8.25 at.% P-containing BMGs, respectively) were prepared by induction melting a mixture of constituent elements with a purity above 99.9%. Ribbons with a thickness of 23 μ m and a width of 1.5 mm were produced by single roller melt-spinning method. Cylindrical rods with diameters of 1–2.5 mm and a length of 30 mm were produced via injection casting into a copper mold. The ϵ_p and σ_y were measured at room temperature by compression measurements with a Sans 5305 testing machine at a strain rate of $5 \times 10^{-4} \text{ s}^{-1}$. The samples were cut from the as-cast glassy rods with a gauge aspect ratio of 2:1 (1 mm in diameter). The toughness of the investigated FeNi-based BMGs was assessed with K_Q under mode I conditions, measured using three-point single edge notched bend (SENB) measurements. Here, we measure conditional (notch) fracture toughness, K_Q , and not K_{IC} for two reasons. First, the inherent critical-casting thickness limitation of these FeNi-based BMGs makes it difficult to obey the standard K_{IC} procedure. Second, the K_Q value is meaningful in distinguishing the variation in toughness of materials under identical testing conditions, and this method has been used in Fe-, Ni- and Mg-based BMGs, which provides a large database for comparison. Note that, the K_Q was obtained using the relation:

$$K_Q = \frac{8PS}{\pi D^3} \sqrt{\pi b} \times F\left(\frac{b}{D}\right) \quad (1)$$

where P is the maximum load, S is the sample span, b is the notch depth, D is the sample diameter, and $F\left(\frac{b}{D}\right)$ is a constant coefficient related to the shape of notch, sample geometry and loading methods (here $F\left(\frac{b}{D}\right) = 1.2$ [30]). The SENB measurements, fixed at 12 mm span, were performed on a CMT 4503 testing machine with a maximum load of 10 kN under displacement control at 0.1 mm/min. Samples for K_Q measurements were taken from the as-cast rods with 1.5 mm in diameter. Notches with a root radius of about 200 μ m were made to a depth of approximately half of the rod diameter via a diamond-cutting machine (SYJ-150). About 10 samples were conducted for each composition in both compression and SENB tests to ensure the results reproducibility. The

morphologies of deformed and fractured surfaces were observed by scanning electron microscopy (SEM, Sirion 200, FEI). Magnetic properties of B_s , H_c , and μ_e were measured with a vibration sample magnetometer (VSM, Lake Shore 7410), a DC $B-H$ loop tracer (RIKEN BHS-40) under a field of 800 A/m, and an impedance analyzer (E4990A) under a field of 1 A/m, respectively. All of the ribbon samples for magnetic property measurements were isothermally annealed at specific temperatures (50 K less than the glass transition temperature) for 600 s in a vacuum chamber in order to reduce the influence of inner stress on soft magnetic properties through structural relaxation. The glass transition temperature (T_g) of the glassy ribbons were measured by differential scanning calorimeter (DSC, NETZSCH 404F3) at a heating rate of 0.67 K/s. The measured T_g values of $\text{Fe}_{39}\text{Ni}_{39}\text{B}_{16.95-x}\text{Si}_{2.75}\text{Nb}_{2.3}\text{P}_x$ ($x = 1.38, 2.75, 4.13, 5.5, 6.88$ and 8.25 at.%) glassy ribbons are 723, 719, 711, 711, 709 and 707 K, respectively. The atomic structure of these FeNi-based metallic glasses was observed by synchrotron XRD using the beam line 11-IDC in the Advanced Photon Source, Argonne National Laboratory, USA. The photon energy was 105.1 keV corresponding to an X-ray wavelength of 0.11798 Å and the beam size was $0.5 \times 0.5 \text{ mm}^2$. The resultant 2D image files were integrated using the Fit2D program to obtain 1D intensity distributions as a function of the wavevector Q [31], from which the $S(Q)$ and the $G(r)$ were derived using the PDFgetX2 program [32]. The high-resolution transmission electron microscope (HRTEM) observations of samples were carried out on an aberration-corrected FEI Titan 80/300 microscope. Samples for HRTEM were prepared by ion milling method (Gatan Inc., PIPS-M691) under liquid nitrogen cooling condition.

3. Results and discussions

3.1. Excellent combination of strength and toughness

The glassy alloy rods were produced at all alloy compositions in this $\text{Fe}_{39}\text{Ni}_{39}\text{B}_{16.95-x}\text{Si}_{2.75}\text{Nb}_{2.3}\text{P}_x$ system. The critical diameters (D_c) of the glassy alloy rods were 1.5, 2, 2.5, 2, 1.5 and 1 mm for alloys with P content of 1.38, 2.75, 4.13, 5.5, 6.88 and 8.25 at.%, respectively, indicating the high GFA of 4.13 at.% P-containing BMG. By using FeNi-based glassy alloy rods with diameters of 1 mm, we measured mechanical properties by compressive test. Fig. 1a shows the compressive stress-strain curves of $\text{Fe}_{39}\text{Ni}_{39}\text{B}_{16.95-x}\text{Si}_{2.75}\text{Nb}_{2.3}\text{P}_x$ BMGs deformed at room temperature. As shown in the figure, the ϵ_p dramatically increases from 5 to 9.8% with P content increasing from 1.38 to 4.13 at.%, then decreases to 1.5% with further increasing P content to 8.25 at.%. In addition, although the σ_y of the samples gradually decreases with increasing P content, all σ_y are larger than 2700 MPa. The SEM image of the lateral surface of deformed 4.13 at.% P-containing BMG is shown in Fig. 1b. Multiple shear bands interconnected by intersection or arrested with each other can be observed, which contributes to the strain-hardening behavior occurring at the initial stage of plastic deformation in the stress-strain curve. Meanwhile, many small kinks, branches, and ledges along the shear bands can be also observed in the region A of Fig. 1b, indicating the excellent resistance ability to the propagation of shear bands. Besides, the inset in Fig. 1b shows the well-developed vein patterns on the fracture surface of 4.13 at.% P-containing BMG, which is a characteristic of large plasticity for ductile BMGs [16,18].

As this FeNi-based BMG system exhibits good mechanical properties with a combination of large plasticity and high strength, as well as multiplane sliding activities during compression, a high toughness can be expected. To evaluate fracture toughness experimentally, the SENB measurements were carried out on the notched 1.38 at.%, 4.13 at.%, and 6.88 at.% P-containing BMG samples. According to the Eq. (1), the K_Q of this FeNi-based BMG system is 44.8, 72.3 and 14.2 $\text{MPa m}^{1/2}$, respectively. Fig. 2a shows a plot of notch toughness K_Q vs. P contents for the three BMGs. As shown in the figure, the K_Q value increases distinctly with P content increasing from 1.38 to 4.13 at.%, and then decreases sharply with further increasing P content to 6.88 at.%. It is to

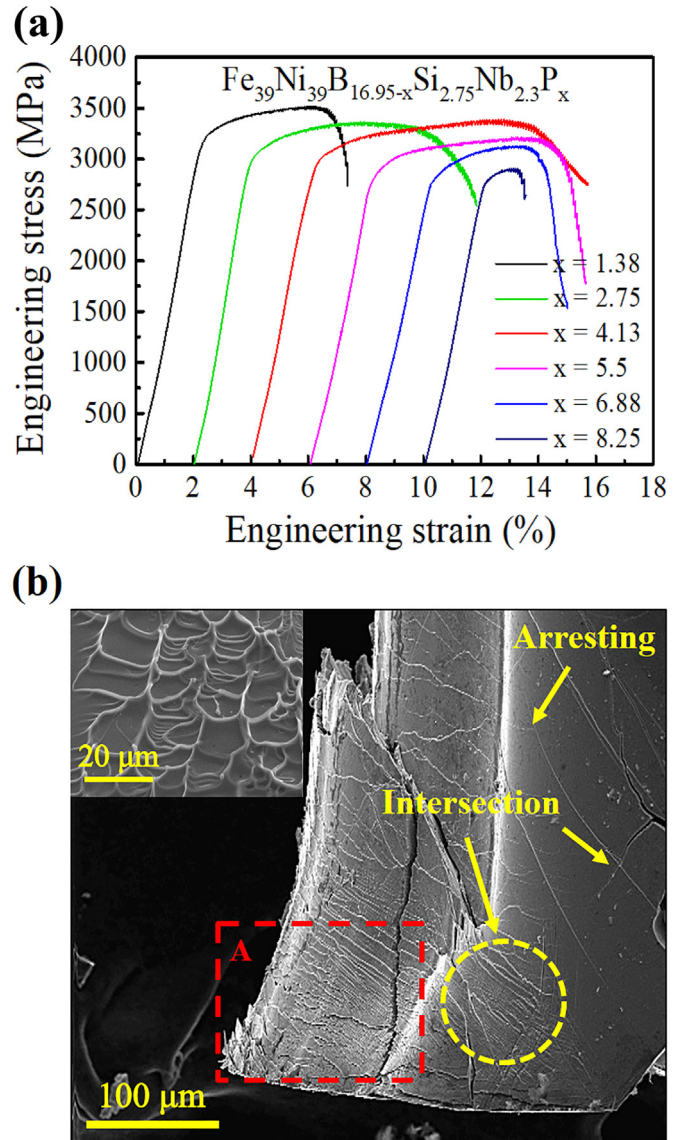


Fig. 1. (a) The compressive stress-strain curves at room temperature of $\text{Fe}_{39}\text{Ni}_{39}\text{B}_{16.95-x}\text{Si}_{2.75}\text{Nb}_{2.3}\text{P}_x$ ($x = 1.38, 2.75, 4.13, 5.5, 6.88$ and 8.25 at.%) BMGs. (b) Deformation surface of the compressed 4.13 at.% P-containing BMG showing multiple shear bands. The inset shows the vein patterns on the fracture surface of failed 4.13 at.% P-containing BMG.

be noted that the large error bar for the toughness value originates from the possible presence of processing defects in samples [33,34], thus, extrinsic effects must be minimized in order to guarantee the reliability of such high toughness. The inset in Fig. 2a is the size and geometry of samples before and after SENB measurements for the 4.13 at.% P-containing BMG, which shows that this notched FeNi-based BMG is capable of undergoing deformation before fracture. In addition, the fracture surface of the 4.13 at.% P-containing BMG exhibits jagged appearance and high roughness under low magnification as shown in Fig. 2b. The inset in Fig. 2b shows very rough characteristic of periodic corrugation pattern zone, which is the enlarged view of region A in Fig. 2b. This high roughness is considered to be caused by the energy dissipation during crack propagation, which means most crack paths in this metallic glass sample are deflected, that is, high energy is needed to break the notched sample, leading to a high toughness.

To compare the mechanical properties of this FeNi-based BMG with those of the other BMG system more detailed, the data of σ_y and toughness (K_C , including K_{IC} and K_Q) of the typical BMG systems are summarized as shown in Fig. 3a. It is clearly seen that nearly all the K_C correlate

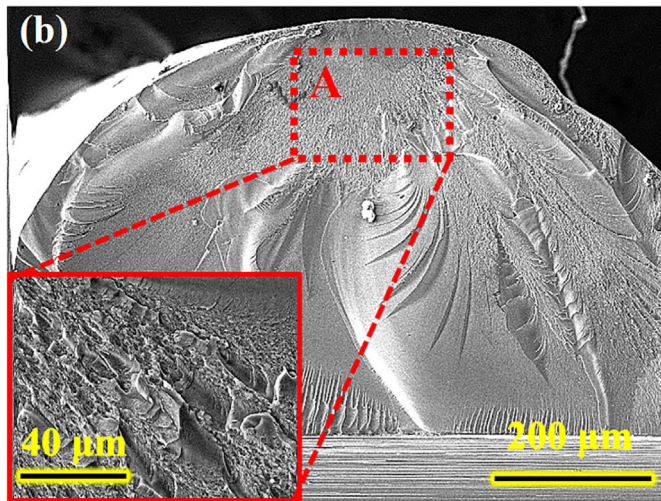
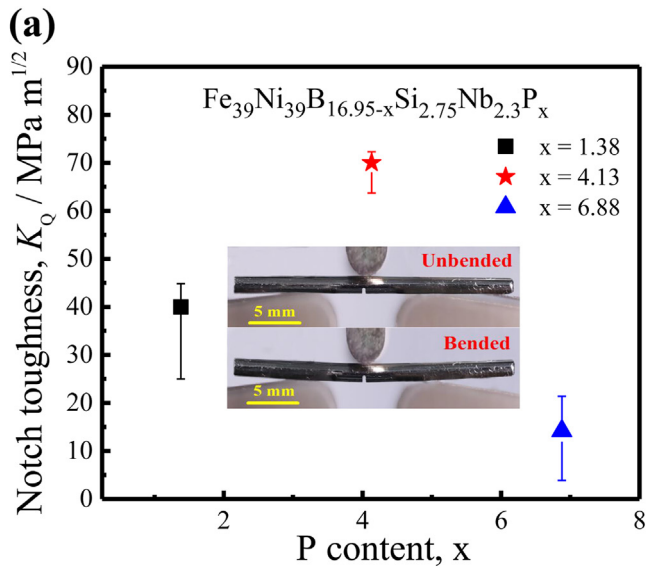


Fig. 2. (a) The notch toughness of 1.38 at.%, 4.13 at.%, and 6.88 at.% P-containing BMGs. The insets show the size and geometry of samples before and after SENB measurements for the 4.13 at.% P-containing BMG. (b) The SEM image of the fracture surface of notched 4.13 at.% P-containing BMG sample after SENB measurement. The inset is the SEM image of high magnification showing region A in (b).

inversely to the σ_y among these BMG systems as illustrated by black dotted curve [2,6–9,19–22,35–41], except for the Mg-based BMG system [42]. The BMG system can be roughly classified into three groups according to their σ_y and K_C correlations separated by red dashed line. For instance, the Mg- and RE-based BMG system with low σ_y and K_C are labeled as Group I. Followed up with Group I, Group II shows high σ_y with high K_C (Pd-, Pt- and Ti-based BMG systems) or relatively high K_C (Zr- and Cu-based BMG systems) combinations. However, as shown in Group III, the Ni- and Fe-based BMG systems exhibit superhigh σ_y but low K_C . It is known that high strength serves as the basis for the applications of structural materials, while the safety must be insured by appropriate toughness [43]. Therefore, it is significant to improve the K_C for the Fe- and Ni-based BMG systems for simultaneously exhibiting high σ_y and K_C . In this study, through adjusting the atomic ratio of P/B elements, the 4.13 at.% P-containing BMG simultaneously exhibits superhigh σ_y of 2930 MPa and high K_C of 72.3 MPa $m^{1/2}$ shown as a red star in Fig. 3a. It is clearly seen that the newly developed 4.13 at.% P-containing BMG in this work is not only the toughest Fe-based BMG, but also a breakthrough of the general

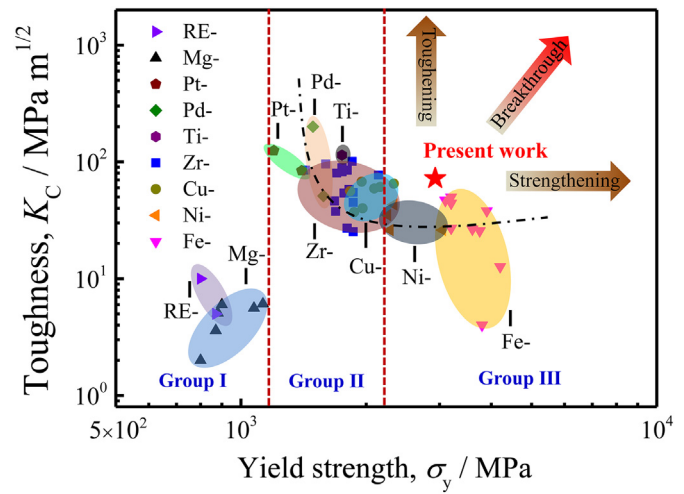


Fig. 3. Relationship between the σ_y and the K_C of the typical BMG systems.

trade-off between σ_y and K_C in BMG family. It is to be noted that the test sample thickness, width, and notch precision strongly effect the fracture toughness of BMGs [44,45], therefore, it is just a rough comparison between this FeNi-based BMG and other Zr-, Pd-, Ti-, Pt-based BMGs. However, for Fe-, Cu-, Ni- and Mg-based BMGs, the K_Q is measured by using the samples with similar configurations and dimensions to the present work, which is suitable for direct comparison.

3.2. Soft magnetic properties

In addition to the good mechanical properties, this FeNi-based metallic glass system exhibits excellent soft magnetic properties as well. Fig. 4a shows the hysteresis loops measured with VSM, and the $B-H$ loops (inset) measured with DC $B-H$ loop tracer for $Fe_{39}Ni_{39}B_{16.95-x}Si_{2.75}Nb_{2.3}P_x$ metallic glasses. It is clear that the B_s decreases gradually from 0.90 to 0.81 T with increasing P content. This is due to the 3 s band electrons from P atoms, which move more easily compared with those 2 s band electrons from B atoms, occupying more unfilled 3d orbits of Fe and Ni atoms. Besides, with an increase of P content from 1.38 to 4.13 at.%, the H_c decreases from 1.2 to 0.65 A/m, and then increases to 1.3 A/m with 8.25 at.% P content, as shown in the inset. The frequency dependence of the permeability under a field of 1 A/m is shown in Fig. 4b and the μ_e at 1 kHz increases from 19,300 to 23,250 with the increase of P content from 1.38 to 4.13 at.%, and then decreases to 19,000 with 8.25 at.% P content, which is in agreement with the change of GFA and H_c . This FeNi-based metallic glass system shows high stability of μ_e upon an increase in frequency. As shown in Fig. 4b, the μ_e for 4.13 at.% P-containing metallic glass, remains as high as 19,080 when the frequency is increased to 10 kHz. Even at 20 kHz, which is just below the cut-off frequency, μ_e remains high at 17370. Especially for 6.88 at.% and 8.25 at.% P-containing metallic glasses, the μ_e hold almost constant values until the cut-up frequency. It is known that the H_c and μ_e are structure sensitive magnetic properties, largely affected by the microstructure. Thus, the highest GFA of 4.13 at.% P-containing metallic glass leads to the highest degree of amorphicity, resulting in the lowest density of domain-wall pinning sites in sample with annealing, then the excellent soft magnetic properties [46]. Another reason is the sufficient release of strain during annealing treatment due to the good GFA and high resistance against crystallization. Additionally, the low saturation magnetostriction constant of FeNi-based glassy alloys plays important roles as well.

Fig. 5 shows the data of H_c , μ_e , and D_c of the 4.13 at.% P-containing metallic glass (marked by a red star) and other representative FeNi-based metallic glasses [17,27,47–52]. As shown in the figure, when compared with the 4.13 at.% P-containing metallic glass, the $Fe_{40}Ni_{40}P_{14}B_6$,

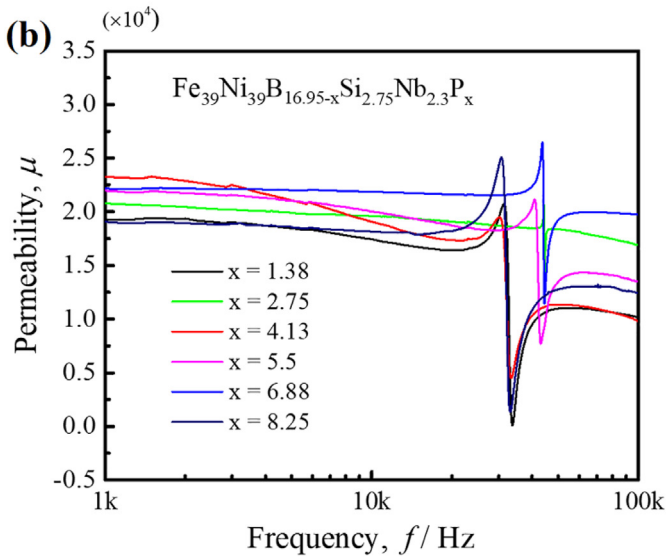
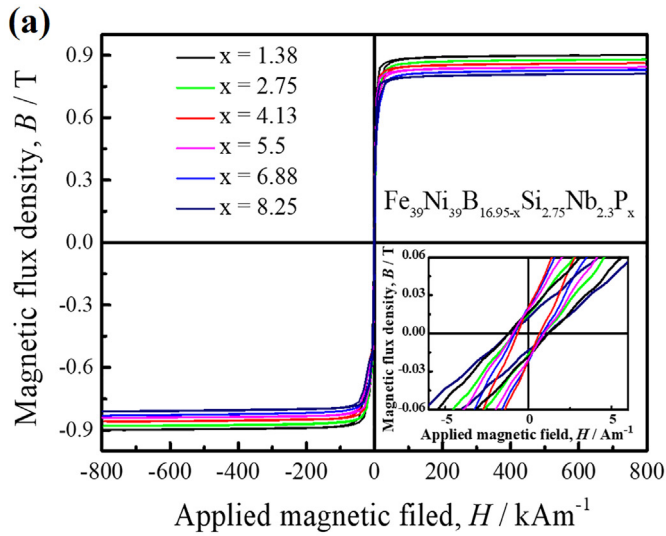


Fig. 4. (a) Hysteresis loops of $\text{Fe}_{39}\text{Ni}_{39}\text{B}_{16.95-x}\text{Si}_{2.75}\text{Nb}_{2.3}\text{P}_x$ ($x = 1.38, 2.75, 4.13, 5.5, 6.88$ and 8.25 at.%) metallic glasses. The insert is the hysteresis curves measured by DC $B-H$ loop tracer. (b) Permeability as a function of applied field frequency for the $\text{Fe}_{39}\text{Ni}_{39}\text{B}_{16.95-x}\text{Si}_{2.75}\text{Nb}_{2.3}\text{P}_x$ ($x = 1.38, 2.75, 4.13, 5.5, 6.88$ and 8.25 at.%) metallic glass ribbons.

$\text{Fe}_{40}\text{Ni}_{38}\text{Mo}_4\text{B}_{18}$, $\text{Fe}_{39}\text{Ni}_{39}\text{Mo}_4\text{Si}_6\text{B}_{12}$, $\text{Fe}_{46}\text{Ni}_{39}\text{Mo}_{3.5}\text{P}_{10}\text{C}_4\text{B}_4\text{Si}_{2.5}$, and $(\text{Fe}_{0.5}\text{Ni}_{0.5})_{75.5}\text{B}_{14.5}\text{P}_7\text{Nb}_3$ metallic glasses [47–50] show relatively lower μ_e of less than 20,000, higher H_c of over 1 A/m, and a smaller D_c of less than 1 mm. For $\text{Fe}_{50}\text{Ni}_{30}\text{P}_{13}\text{C}_7$ [17,51] and $(\text{Fe}_{0.5}\text{Ni}_{0.5})_{0.78}\text{B}_{0.17}\text{P}_{0.05}\text{Nb}_3$ [27] metallic glasses, although they show higher μ_e , but their H_c is higher and GFA remains limited. It is thus concluded that the 4.13 at.% P-containing metallic glass exhibits extremely low H_c of 0.65 A/m, high μ_e of 23,250 with high frequency stability, and a high GFA among FeNi-based metallic glass family.

3.3. The origin of high toughness

To shed light onto the origin of high toughness of the 4.13 at.% P-containing BMG from a structural perspective, synchrotron XRD measurements were carried out. Fig. 6a shows the total synchrotron XRD structure factor $S(Q)$ of the 1.38 at.%, 4.13 at.%, and 6.88 at.% P-containing metallic glasses. For more clarity, the encircled part of the first peak for every metallic glass in Fig. 6a was enlarged respectively as shown in Fig. 6b, and the dashed line denotes the peak position (Q_1). It can be seen that the Q_1 decreases rapidly from 3.118 to 3.107 \AA^{-1} with P increasing from 1.38 to 4.13 at.%, then decreases

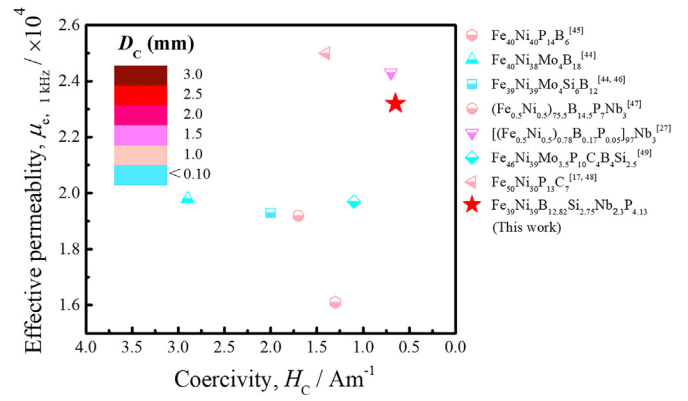


Fig. 5. Comparison of H_c , μ_e and D_c for the 4.13 at.% P-containing metallic glass (marked by a red star) and other representative FeNi-based metallic glasses. (For interpretation of the references to color in this figure legend, the reader is referred to the web version of this article.)

slowly to 3.105 \AA^{-1} with further increasing P to 6.88 at.%. As Q_1 is inversely proportional to the mean atomic distance [53], a smaller Q_1 of 4.13 at.% P-containing metallic glass corresponds to a larger mean atomic distance when compared with the 1.38 at.% P-containing metallic glass. The change in mean atomic volume with P changing from 1.38 to 4.13 at.% can be estimated from Eq. (2) as below [54]:

$$V_{x=1.38}/V_{x=4.13} = (Q_{x=4.13}/Q_{x=1.38})^3 \quad (2)$$

where $V_{x=1.38}$ and $V_{x=4.13}$ is the mean atomic volumes of 1.38 at.% and 4.13 at.% P-containing metallic glasses, respectively, and $Q_{x=1.38}$ and $Q_{x=4.13}$ are their peak positions, respectively. As a result, the atomic volume of 4.13 at.% P-containing metallic glass is 1% larger than that of 1.38 at.% P-containing metallic glass, indicating a significant increase in free volume due to the increase of P/B atomic ratio. In addition, it should be mentioned that the change in atomic volume with P further increasing from 4.13 to 6.88 at.% is extremely small.

It is known that the deformation in BMGs is related to the cooperative rearrangement of atomic clusters under the applied shear stress at room temperature, termed shear transformation zones (STZs). Such zones are closely associated with free volume, which is defined as the atomic volume in excess of the ideal structure [55]. Previous studies have found that the large plasticity of BMGs is associated with the large amount of free volume [56–58], which can be explained based on the following three points of view [56,59–63]. Firstly, the large amount of free volume provides more potential STZ sites for initial nucleation and branching of shear bands. Concurrent nucleation and branching of multiple shear bands restrict the dominant shearing process. Secondly, the large amount of free volume means high atomic diffusion ability. The atomic rearrangement processes can be accelerated and release the stress at the crack tip through viscous flow and even lead to the healing of minor cracks, which increases the fracture energy and deflection of crack path in the sample with large free volume. Thirdly, more free volume indicates more loosely packed structure. Previous reports have shown that more loosely packed metallic glasses are more prone to particle rearrangements and energy loss during shearing, and the enhanced energy loss through particle rearrangements at small strains can prevent catastrophic brittle failure, by preventing stress accumulation and localization [61–63]. Thus, the 4.13 at.% P-containing BMG with a relatively large free volume having a large amount of multiple shear bands on the deformed zone, which results in the large roughness on the fracture surface, as shown in Fig. 2b. The increasing free volume with increase of P/B atomic ratio could be attributed to the replacement of B atoms (0.078 nm) by larger P atoms (0.115 nm) [64], leading to the expansion of atomic scale structure.

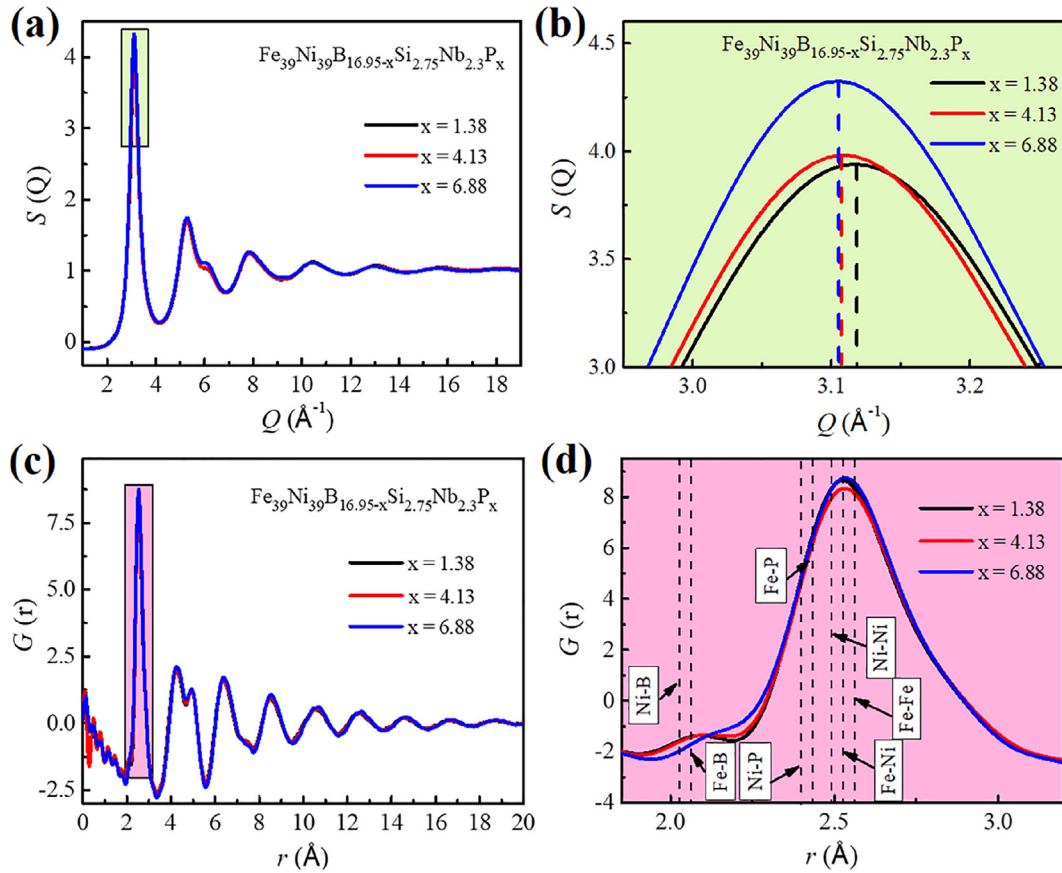


Fig. 6. The synchrotron XRD results of 1.38 at.%, 4.13 at.%, and 6.88 at.% P-containing metallic glasses. (a) Total structure factor $S(Q)$. (b) Enlarged regions on the first peaks of $S(Q)$ shown in (a) with dashed lines denoting the peak positions. (c) Reduced pair distribution function $G(r)$. (d) Enlarged region on the first nearest neighbor peaks of $G(r)$ function shown in (c) with dashed lines denoting atomic bond length shown in Table 1.

To further investigate the structural evolution of the samples with different P content, the reduced pair distribution functions ($G(r)$) were derived from $S(Q)$ as shown in Fig. 6c. It can be seen that the peaks of the first coordination shell for the three metallic glasses are located at around 2.53 Å due to the dominant atomic pairs of Fe—Ni, Ni—Ni and Fe—Fe. The encircled part of the first peak for three samples corresponding to the first nearest neighbor shell of atoms (1.85–3.2 Å) was also enlarged respectively as shown in Fig. 6d, and the peak position for the 1.38 at.%, 4.13 at.%, and 6.88 at.% P-containing BMG locates at 2.525 Å, 2.530 Å, and 2.535 Å, respectively. Based on the atomic radii of each constituent in FeNiBSiPnB BMGs [64], the values of interatomic atomic bond lengths (r_{ij}) were calculated, as shown in Table 1, and the major ones, denoted by dashed lines, were added in Fig. 6d. Table 1 also lists the corresponding X-ray weighting factor (w_{ij} , calculated at $Q = 0 \text{ \AA}^{-1}$) [65] of three metallic glasses, which is the nominal content of each atomic pair. It can be seen from the table that the w_{ij} decreases gradually for Fe—B and Ni—B bonds and increases significantly for Fe—P and Ni—P bonds with increasing P content. Besides, as shown in Fig. 6d, there is a small pre-peak locating at $r \approx 2.1 \text{ \AA}$ for the 1.38 at.% and 4.13 at.% P-containing metallic glasses. The amplitude of this peak decreases with increasing P content, due to the decrease of w_{ij} for Fe—B and Ni—B bonds. However, the location of the first peak does not shift to Fe—P and Ni—P bond positions, but it shifts closer towards the Ni—Ni, Fe—Ni and Fe—Fe bond positions, indicating that the interatomic bond in this metallic glass system tends to change from metal-metalloid (Fe—B, Ni—B, Fe—P and Ni—P) to metal-metal bond (Fe—Fe, Ni—Ni and Fe—Ni) with increasing P content. These interatomic bonds in atomic configurations could also influence the plasticity of Fe-based BMGs [17,28,66]. It has been reported that Fe-based BMGs containing metalloids with less directional metal-metalloid bonds and

more non-directional metal-metal bonds show larger plasticity [17], because the metal-metal connecting region is more likely to be deformed plastically, since shear bands are preferentially formed and activated in regions involving weakly bonded atoms [67]. Thus, the transformation

Table 1

Values of the theoretical interatomic bond length (r_{ij} , sum of the Goldschmidt radii) and the corresponding X-ray weighting factor (w_{ij} , calculated at $Q = 0 \text{ \AA}^{-1}$).

Atomic pair ij	r_{ij} (Å)	w_{ij}		
		1.38 at.% P-containing metallic glass	4.13 at.% P-containing metallic glass	6.88 at.% P-containing metallic glass
Fe-Fe	2.56	0.188	0.184	0.180
Fe-Ni	2.53	0.405	0.396	0.387
Ni-Ni	2.50	0.218	0.213	0.208
Fe-B	2.06	0.029	0.023	0.018
Fe-P	2.43	0.008	0.022	0.037
Fe-Si	2.30	0.014	0.014	0.014
Ni-B	2.03	0.031	0.025	0.019
Ni-P	2.40	0.008	0.024	0.039
Ni-Si	2.27	0.015	0.015	0.015
Fe-Nb	2.74	0.035	0.034	0.033
Ni-Nb	2.71	0.038	0.037	0.036
B-B	1.56	0.001	0.001	0.001
B-Si	1.80	0.001	0.001	0.001
B-P	1.93	0.001	0.001	0.001
B-Nb	2.24	0.003	0.002	0.002
Si-Si	2.04	0.0003	0.0003	0.0003
Si-P	2.17	0.0003	0.0008	0.0014
Si-Nb	2.48	0.001	0.001	0.001
P-P	2.30	0.0001	0.0007	0.0018
P-Nb	2.61	0.0007	0.0021	0.0034
Nb-Nb	2.92	0.002	0.002	0.002

from metal-metalloid bonds to metal-metal bonds with increasing P content in this study for the $\text{Fe}_{39}\text{Ni}_{39}\text{B}_{16.95-x}\text{Si}_{2.75}\text{Nb}_{2.3}\text{P}_x$ BMG system indicates that adjusting the P/B atomic ratio can effectively change the atomic bonding nature, leading to improve its plasticity.

Previous work shows that the toughness of BMGs results from a competition between the plastic relaxation timescale (τ_{plastic}), which is inversely proportional to the density of plasticity carriers (i.e., STZs), and an effective loading timescale near the notch root (τ_e), which depends on the applied strain rate and local stress [68,69]. High toughness is usually related to low τ_{plastic} and high τ_e . In this work, the applied strain rate and local stresses (set by the sample's geometry and the external loading) are identical, indicating that the τ_e is a definite value. Besides, the higher P-containing BMG contains more free volume and metal-metal bonds, resulting in more potential STZ sites, thereby the lower τ_{plastic} . Thus, the higher-P containing BMG should exhibit improved toughness. However, compared with the 4.13 at.% P-containing BMG, the 6.88 at.% P-containing BMG has similar content of free volume and more metal-metal bonds but shows low toughness. It seems that free volume and atomic bonding nature are not the only influence factor affecting the deformation and fracture behaviors of this FeNi-based BMG system. Here, structural disorder degree which is inversely proportional to the fractions of the various short-range scale clusters or the degree of short-to-medium range orderings [70,71] should be also considered. As shown in Fig. 6c, the intensity of $G(r)$ maxima for the 1.38 at.% and 6.88 at.% P-containing metallic glasses are higher than that for the 4.13 at.% P-containing metallic glass, while a reverse behavior is observed for the $G(r)$ minima. Furthermore, the $\Delta G(r)_1 = G(r)_{x=6.88} - G(r)_{x=4.13}$ and $\Delta G(r)_2 = G(r)_{x=1.38} - G(r)_{x=4.13}$ was calculated and plotted in Fig. 7. As shown in the figure, both curves show positive and negative values at positions of $G(r)$ maxima and minima, respectively, indicating that the diffraction maxima and minima exhibit an opposite behavior with the 4.13 at.% P content. In other words, compared with the 1.38 at.% and 6.88 at.% P-containing metallic glasses, the intensity of the diffraction maximum decreases, while that of diffraction minima increases in the 4.13 at.% P-containing metallic glass. These results show that the $G(r)_{x=4.13}$ peaks are the broadest, reflecting the least pronounced topological ordering, which indicates that the 4.13 at.% P-containing metallic glass has the highest structural disorder than the other two metallic glasses.

Besides, to further understand the effects of structural disorder on the toughness of this FeNi-based BMG system, the HRTEM observation was also carried out. Fig. 8a and b show the typical HRTEM image and selected area electron diffraction (SAED) pattern of the 4.13 at.% and 6.88 at.% P-containing BMGs. It can be seen that both the samples

keep the amorphous structure with different P/B atomic ratio, but the atomic-scale ordering are different. The Fast-Fourier-Transformation (FFT) and inverse Fast-Fourier-Transformation (IFFT) were conducted on the selected areas shown as yellow box in Fig. 8a and b to reveal such a difference. As shown in Fig. 8c and d, local lattice fringes can be observed in both the samples, indicating that there are regions with crystal-like order (CLO) in the amorphous matrix [72]. FFT patterns of selected regions show bright spots (indicated by white circles) on the broad halo, confirming the presence of these CLO regions as shown in the insets of Fig. 8c and d. All the CLO regions observed in the 4.13 at.% P-containing BMG sample are in the size ranging from 0.5–1 nm and dispersed homogeneously in the amorphous matrix. However, the CLO region with a large size of 3 nm can be observed in the 6.88 at.% P-containing BMG sample. The small scale of CLO regions in the 4.13 at.% P-containing BMG sample agrees well with its high structural disorder degree measured by synchrotron XRD experiments.

It can be seen from the HRTEM image that the local structural heterogeneity of this FeNi-based BMG system increased with increasing the P/B atomic ratio, which is due to the mutual repulsion of B–P atomic pair. However, more addition of P element caused to increase the size of CLO region. Thus, the 4.13 at.% P-containing BMG with uniformly distributed CLO regions in size of 0.5–1 nm exhibits the highest structural disorder degree. It has been demonstrated that STZs preferentially nucleate in the more disordered regions where the local stiffness and stability are low, while highly-ordered clusters constitute the main resistance for plastic flow in BMGs [73,74]. Therefore, in 4.13 at.% P-containing BMG, the STZs initiate at the more disordered areas between CLO regions, then the subsequently propagation of shear bands are hindered by these CLO regions. Because of the uniformly spread CLO regions throughout the amorphous matrix, homogeneously distributed nucleation and hindrance sites of STZs tend to link shear bands to form a continuous network, preventing the primary shear bands from developing into cracks quickly, which has been also observed in the $\text{Fe}_{50}\text{Ni}_{30}\text{P}_{13}\text{C}_7$ BMG reported by Sarac et al. [18]. Nevertheless, for BMGs with lower structural disorder degree, stress concentration occurs around the larger CLO regions, and numerous STZs cluster in a certain narrow belt and quickly form a macroscopic crack, which results in a catastrophic fracture.

4. Conclusion

According to the theory of structural inhomogeneity in BMGs, a tough $\text{Fe}_{39}\text{Ni}_{39}\text{B}_{12.82}\text{Si}_{2.75}\text{Nb}_{2.3}\text{P}_{4.13}$ BMG with diameter up to 2.5 mm was successfully developed by adjusting the P/B atomic ratio of FeNiSiNbP BMG system. This novel FeNi-based BMG simultaneously exhibits excellent mechanical and soft magnetic properties, i.e., high K_Q of 72.3 $\text{MPa m}^{1/2}$, large ε_p of 9.8%, high σ_y of 2930 MPa, extremely low H_c of 0.65 A/m, and high μ_e of 23,250 with high frequency stability. The toughness of this FeNi-based BMG is the highest value among Fe-based BMGs reported to date, and this excellent combination of high toughness and high strength is a breakthrough of the general trade-off between σ_y and K_C in BMG family. Based on the analyses from the change in atomic structure, the high toughness is attributed to the high content of free volume and metal-metal bonds, as well as high structural disorder degree, which lead to a large number of potential STZ sites. Among them, the high structural disorder degree plays a key role, since homogeneously distributed CLO regions with the size of 0.5–1 nm hinder the propagation of STZs, resulting in the interaction of shear bands and the large deflection of crack path. The new FeNi-based BMG with excellent comprehensive performance is promising for future development as a new structural and functional material, and this study also gives us a guideline to develop tough FeNi-based BMGs combined with high strength and excellent soft magnetic properties.

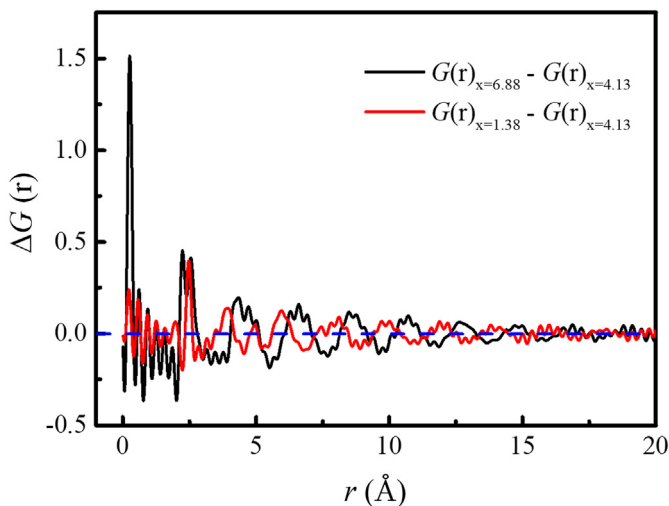


Fig. 7. The difference curves for: (a) $\Delta G(r)_1 = G(r)_{x=6.88} - G(r)_{x=4.13}$, and (b) $\Delta G(r)_2 = G(r)_{x=1.38} - G(r)_{x=4.13}$.

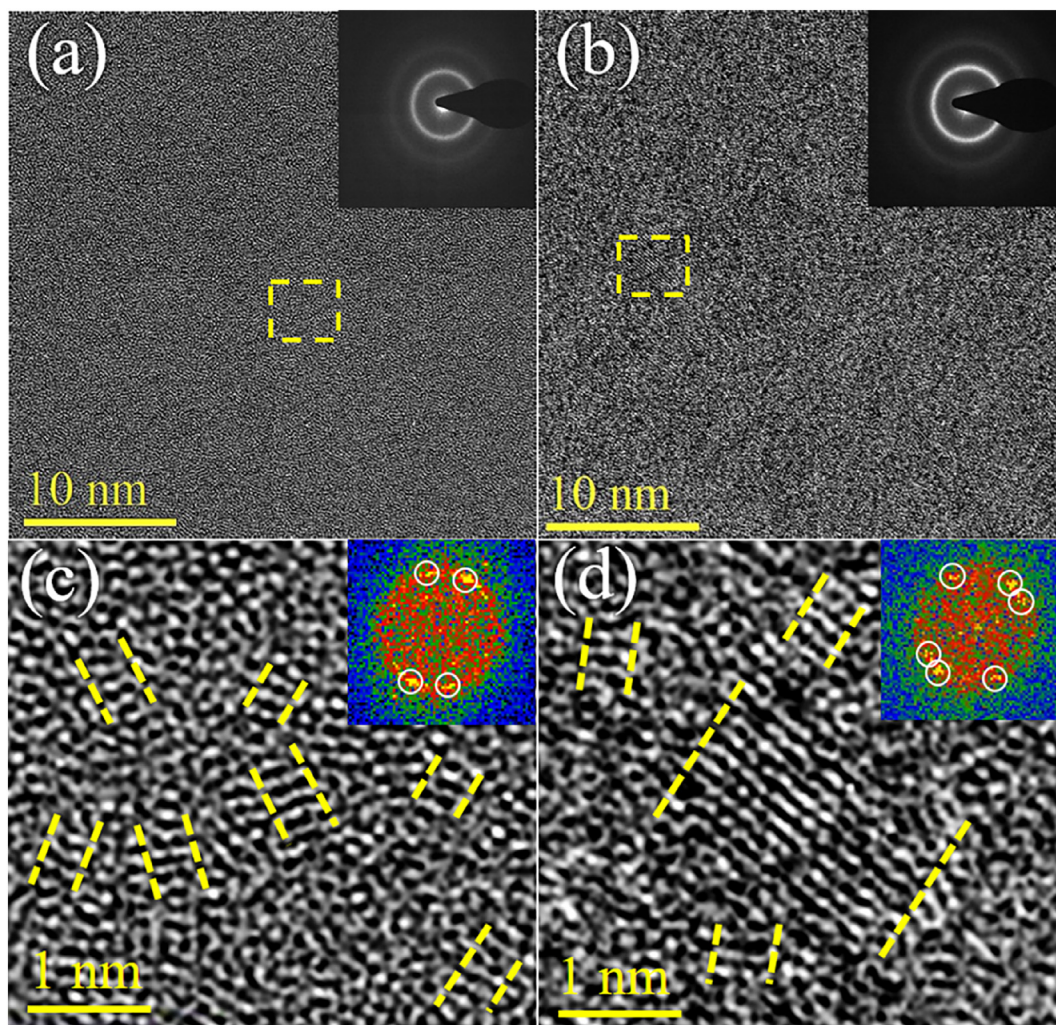


Fig. 8. The HRTEM images with the corresponding SAED patterns in the insets for (a) 4.13 at.% P-containing BMG and (b) 6.88 at.% P-containing BMG. (c) and (d) are the IFFT-filtered images with the FFT patterns in the insets of the yellow square areas in (a) and (b). (For interpretation of the references to color in this figure legend, the reader is referred to the web version of this article.)

CRediT authorship contribution statement

Jing Zhou: Data curation, Investigation, Writing - original draft, Writing - review & editing. **Qianqian Wang:** Writing - original draft. **Xidong Hui:** Resources. **Qiaoshi Zeng:** Investigation. **Yuwei Xiong:** Investigation. **Kuibo Yin:** Resources. **Baoan Sun:** Formal analysis, Writing - review & editing. **Litao Sun:** Resources. **Mihai Stoica:** Writing - original draft. **Weihua Wang:** Methodology. **Baolong Shen:** Conceptualization, Funding acquisition, Project administration, Supervision, Writing - original draft, Writing - review & editing.

Declaration of competing interest

We declare that we have no financial and personal relationships with other people or organizations that can inappropriately influence our work, there is no professional or other personal interest of any nature or kind in any product, service and/or company that could be construed as influencing the position presented in, or the review of, the manuscript entitled.

Acknowledgements

This work was supported by the National Natural Science Foundation of China (Grant Nos. 51631003, 51871054 and 51571016), and the Fundamental Research Funds for the Central Universities (Grant

Nos. 2242019k1G005 and 2242019K40183). This research used the beamline 11-ID-C at APS, ANL, USA. APS is supported by the Department of Energy (DOE) Office of Science (DE-AC02-06CH11357).

References

- [1] C.A. Schuh, T.C. Hufnagel, U. Ramamurty, Mechanical behavior of amorphous alloys, *Acta Mater.* 55 (2007) 4067–4109.
- [2] M.D. Demetriou, M.E. Launey, G. Garrett, J.P. Schramm, D.C. Hofmann, W.L. Johnson, R.O. Ritchie, A damage-tolerant glass, *Nat. Mater.* 10 (2011) 123–128.
- [3] J. Schroers, W.L. Johnson, Ductile bulk metallic glass, *Phys. Rev. Lett.* 93 (2004), 255506.
- [4] D.C. Hofmann, J.Y. Suh, A. Wiest, G. Duan, M.L. Lind, M.D. Demetriou, W.L. Johnson, Designing metallic glass matrix composites with high toughness and tensile ductility, *Nature* 451 (2008) 1085–1090.
- [5] M.E. Launey, D.C. Hofmann, J.Y. Suh, H. Kozachkov, W.L. Johnson, R.O. Ritchie, Fracture toughness and crack-resistance curve behavior in metallic glass-matrix composites, *Appl. Phys. Lett.* 94 (2009), 241910.
- [6] X.J. Gu, S.J. Poon, G.J. Shiflet, J.J. Lewandowski, Compressive plasticity and toughness of a Ti-based bulk metallic glass, *Acta Mater.* 58 (2010) 1708–1720.
- [7] Q. He, J.K. Shang, E. Ma, J. Xu, Crack-resistance curve of a Zr-Ti-Cu-Al bulk metallic glass with extraordinary fracture toughness, *Acta Mater.* 60 (2012) 4940–4949.
- [8] S. Evertz, I. Kirchlechner, R. Soler, C. Kirchlechner, P. Kontis, J. Bednarcik, B. Gault, G. Dehm, D. Raabe, J.M. Schneider, Electronic structure based design of thin film metallic glasses with superior fracture toughness, *Mat. Des.* 186 (2020) 108327.
- [9] J. Xu, E. Ma, Damage-tolerant Zr-Cu-Al-based bulk metallic glasses with record-breaking fracture toughness, *J. Mater. Res.* 29 (2014) 1489–1499.
- [10] C. Suryanarayana, A. Inoue, Iron-based bulk metallic glasses, *Int. Mater. Rev.* 58 (2013) 131–166.
- [11] H.X. Li, Z.C. Lu, S.L. Wang, Y. Wu, Z.P. Lu, Fe-based bulk metallic glasses: glass formation, fabrication, properties and applications, *Prog. Mater. Sci.* 103 (2019) 235–318.

- [12] A. Inoue, B.L. Shen, A new Fe-based bulk glassy alloy with outstanding mechanical properties, *Adv. Mater.* 16 (2004) 2189–2192.
- [13] A. Inoue, B.L. Shen, C.T. Chang, Super-high strength of over 4000 MPa for Fe-based bulk glassy alloys in $[(\text{Fe}_{1-x}\text{Co}_x)_{0.75}\text{B}_{0.2}\text{Si}_{0.05}]_{96}\text{Nb}_4$ system, *Acta Mater.* 52 (2004) 4093–4099.
- [14] K.F. Yao, C.Q. Zhang, Fe-based bulk metallic glass with high plasticity, *Appl. Phys. Lett.* 90 (2007), 61901.
- [15] J.M. Park, D.H. Kim, J. Eckert, Enhanced plasticity of Fe-Nb-B-(Ni, Cu) bulk metallic glasses by controlling the heterogeneity and elastic constants, *J. Alloys Compd.* 536 (2012) S70–S73.
- [16] S.F. Guo, J.L. Qiu, P. Yu, S.H. Xie, W. Chen, Fe-based bulk metallic glasses: brittle or ductile? *Appl. Phys. Lett.* 105 (2014), 161901.
- [17] W.M. Yang, H.S. Liu, Y.C. Zhao, A. Inoue, K.M. Jiang, J.T. Huo, H.B. Ling, Q. Li, B.L. Shen, Mechanical properties and structural features of novel Fe-based bulk metallic glasses with unprecedented plasticity, *Sci. Rep.* 4 (2014) 6233.
- [18] B. Sarac, Y.P. Ivanov, A. Chuvilin, T. Schöberl, M. Stoica, Z. Zhang, J. Eckert, Origin of large plasticity and multiscale effects in iron-based metallic glasses, *Nat. Commun.* 9 (2018) 1333.
- [19] P.A. Hess, S.J. Poon, G.J. Shiflet, R.H. Dauskardt, Indentation fracture toughness of amorphous steel, *J. Mater. Res.* 20 (2005) 783–786.
- [20] N.A. Shamimi, X.J. Gu, S.J. Poon, G.J. Shiflet, J.J. Lewandowski, Chemistry (intrinsic) and inclusion (extrinsic) effects on the toughness and Weibull modulus of Fe-based bulk metallic glasses, *Phil. Mag. Lett.* 88 (2008) 853–861.
- [21] J.J. Lewandowski, X.J. Gu, N.A. Shamimi, S.J. Poon, G.J. Shiflet, Tough Fe-based bulk metallic glasses, *Appl. Phys. Lett.* 92 (2008) 91918.
- [22] M.D. Demetriou, G. Kaltenboeck, J. Suh, G. Garrett, M. Floyd, C. Crewdson, D.C. Hofmann, H. Kozachkov, A. Wiest, J.P. Schramm, W.L. Johnson, Glassy steel optimized for glass-forming ability and toughness, *Appl. Phys. Lett.* 95 (2009), 41907.
- [23] S.F. Guo, K.C. Chan, L. Liu, Notch toughness of Fe-based bulk metallic glass and composites, *J. Alloys Compd.* 509 (2011) 9441–9446.
- [24] T. Wang, Y.D. Wu, J.J. Si, Y.H. Liu, X.D. Hui, Plasticizing and work hardening in phase separated Cu-Zr-Al-Nb bulk metallic glasses by deformation induced nanocrystallization, *Mat. Des.* 142 (2018) 74–82.
- [25] R. Hasegawa, Applications of amorphous magnetic alloys, *Mater. Sci. Eng. A* 375–377 (2004) 90–97.
- [26] C.H. Shek, G.M. Lin, K.L. Lee, J.K.L. Lai, Fractal fracture of amorphous FeNiVSiB alloy, *J. Non-Cryst. Solids* 224 (1998) 244–248.
- [27] A.D. Wang, Q.K. Man, M.X. Zhang, H. Men, B.L. Shen, S.J. Pang, T. Zhang, Effect of B to P concentration ratio on glass-forming ability and soft-magnetic properties in $[(\text{Fe}_{0.5}\text{Ni}_{0.5})_{0.78}\text{B}_{0.22-x}\text{P}_x]_{97}\text{Nb}_3$ glassy alloys, *Intermetallics* 20 (2012) 93–97.
- [28] J. Zhou, W.M. Yang, C.C. Yuan, B.A. Sun, B.L. Shen, Ductile FeNi-based bulk metallic glasses with high strength and excellent soft magnetic properties, *J. Alloys Compd.* 742 (2018) 318–324.
- [29] A. Takeuchi, A. Inoue, Classification of bulk metallic glasses by atomic size difference, heat of mixing and period of constituent elements and its application to characterization of the main alloying element, *Mater. Trans.* 46 (2005) 2817–2829.
- [30] Y. Murakami, *Stress Intensity Factors Handbook*, Pergamon, Oxford, United Kingdom, 1987.
- [31] A.P. Hammarsley, S.O. Svensson, M. Hanfland, A.N. Fitch, D. Hausermann, Two-dimensional detector software: from real detector to idealised image or two-theta scan, *High Pressure Res.* 14 (1996) 235–248.
- [32] I.K. Jeong, J. Thompson, T. Proffen, A. Perez, S.J.L. Billinge, PDFgetX: a program for obtaining the atomic pair distribution function from X-ray powder diffraction data, *J. Appl. Crystallogr.* 34 (2001) 536.
- [33] J. Xu, U. Ramamurty, E. Ma, The fracture toughness of bulk metallic glasses, *Jom* 62 (2010) 10–18.
- [34] W. Chen, J. Ketkaew, Z. Liu, R.M.O. Mota, K. O'Brien, C.S. da Silva, J. Schroers, Does the fracture toughness of bulk metallic glasses scatter? *Scripta Mater* 107 (2015) 1–4.
- [35] J.J. Lewandowski, W.H. Wang, A.L. Greer, Intrinsic plasticity or brittleness of metallic glasses, *Phil. Mag. Lett.* 85 (2005) 77–87.
- [36] D.H. Bae, S.W. Lee, J.W. Kwon, X.D. Wang, S. Yi, Ductile Zr-base bulk metallic glass, *Mater. Sci. Eng. A* 449–451 (2007) 111–113.
- [37] C.P. Kim, J. Suh, A. Wiest, M.L. Lind, R.D. Conner, W.L. Johnson, Fracture toughness study of new Zr-based be-bearing bulk metallic glasses, *Scripta Mater* 60 (2009) 80–83.
- [38] P. Jia, Z. Zhu, E. Ma, J. Xu, Notch toughness of Cu-based bulk metallic glasses, *Scripta Mater* 61 (2009) 137–140.
- [39] Q. He, Y. Cheng, E. Ma, J. Xu, Locating bulk metallic glasses with high fracture toughness: chemical effects and composition optimization, *Acta Mater.* 59 (2011) 202–215.
- [40] Z. Zhu, P. Jia, J. Xu, Optimization for toughness in metalloid-free Ni-based bulk metallic glasses, *Scripta Mater* 64 (2011) 785–788.
- [41] S.V. Madge, D.V. Louzguine-Luzgin, J.J. Lewandowski, A.L. Greer, Toughness, extrinsic effects and poisson's ratio of bulk metallic glasses, *Acta Mater.* 60 (2012) 4800–4809.
- [42] S.G. Wang, L.L. Shi, J. Xu, Mg-based bulk metallic glasses: elastic properties and their correlations with toughness and glass transition temperature, *J. Mater. Res.* 26 (2011) 923–933.
- [43] M.F. Ashby, *Materials Selection in Mechanical Design*, Butterworth Heinemann, Oxford, 2011.
- [44] W. Chen, Z. Liu, J. Ketkaew, R.M.O. Mota, S.H. Kim, M. Power, W. Samela, J. Schroers, Flaw tolerance of metallic glasses, *Acta Mater.* 107 (2016) 220–228.
- [45] W. Chen, H.F. Zhou, Z. Liu, J. Ketkaew, L. Shao, N. Li, P. Gong, W. Samela, H.J. Gao, J. Schroers, Test sample geometry for fracture toughness measurements of bulk metallic glasses, *Acta Mater.* 145 (2018) 477–487.
- [46] T. Bitoh, A. Makino, A. Inoue, Origin of low coercivity of $(\text{Fe}_{0.75}\text{B}_{0.15}\text{Si}_{0.10})_{(100-x)}\text{Nb}_x$ ($x = 1-4$) glassy alloys, *J. Appl. Phys.* (8) (2006) 08F102.
- [47] A.D. Wang, M.X. Zhang, J.H. Zhang, H. Men, B.L. Shen, S.J. Pang, T. Zhang, FeNiPBn bulk glassy alloys with good soft-magnetic properties, *J. Alloys Compd.* 536S (2012) S354–S358.
- [48] T.D. Shen, R.B. Schwarz, Bulk ferromagnetic glasses in the Fe-Ni-P-B system, *Acta Mater.* 49 (2001) 837–847.
- [49] T. Komatsu, R. Yokota, T. Shindo, K. Matusita, Study of short-range ordering during structural relaxation in Fe-Ni-Si-B metallic glasses, *J. Non-Cryst. Solids* 65 (1984) 63–71.
- [50] A.D. Wang, M.X. Zhang, J.H. Zhang, H. Men, B.L. Shen, S.J. Pang, T. Zhang, Effect of Ni addition on the glass-forming ability and soft-magnetic properties of FeNiPBn metallic glasses, *Chin. Sci. Bull.* 56 (2011) 3932–3936.
- [51] Q.L. Liu, H.S. Liu, M.Z. Wang, Y. Zhang, Z.G. Ma, Y.C. Zhao, W.M. Yang, Effects of Ni substitution for Fe on magnetic properties of $\text{Fe}_{80-x}\text{Ni}_x\text{P}_{13}\text{C}_7$ ($x = 0-30$) glassy ribbons, *J. Non-Cryst. Solids* 463 (2017) 68–71.
- [52] M.X. Zhang, A.D. Wang, B.L. Shen, Enhancement of glass-forming ability of Fe-based bulk metallic glasses with high saturation magnetic flux density, *AIP Adv.* 2 (2012), 22169.
- [53] A.R. Yavari, A.L. Moulec, A. Inoue, N. Nishiyama, N. Lupu, E. Matsubara, W.J. Botta, G. Vaughan, M.D. Michiel, A. Kvick, Excess free volume in metallic glasses measured by X-ray diffraction, *Acta Mater.* 53 (2004) 1611–1619.
- [54] A.R. Yavari, M. Tonegaru, N. Lupu, A. Inoue, E. Matsubara, G. Vaughan, A. Kvick, W.J. Botta, Quenched-in free volume V_f , deformation-induced free volume, the glass transition T_g and thermal expansion in glassy ZrNbCuNiAl measured by time-resolved diffraction in transmission, *Mater. Res. Soc. Symp. Proc.* 806 (2003) 203.
- [55] F. Spaepen, A microscopic mechanism for steady state inhomogeneous flow in metallic glasses, *Acta Metall.* 25 (1977) 407–415.
- [56] L.Y. Chen, A.D. Setyawan, H. Kato, A. Inoue, G.Q. Zhang, J. Saida, X.D. Wang, Q.P. Cao, J.Z. Jiang, Free-volume-induced enhancement of plasticity in a monolithic bulk metallic glass at room temperature, *Scripta Mater* 59 (2008) 75–78.
- [57] X. Wang, Q.P. Cao, Y.M. Chen, K. Hono, C. Zhong, Q.K. Jiang, X.P. Nie, L.Y. Chen, X.D. Wang, J.Z. Jiang, A plastic Zr-Cu-Ag-Al bulk metallic glass, *Acta Mater.* 59 (2011) 1037–1047.
- [58] Y. Hu, H.H. Yan, J.F. Li, Y.H. Zhou, Bending plasticity of $\text{Zr}_{75}\text{Al}_{10}\text{Ni}_5\text{Cu}_{30}$ bulk metallic glass with monolithic amorphous structure, *J. Alloys Compd.* 688 (2016) 620–625.
- [59] F. Jiang, Y.L. Zhao, L.C. Zhang, S.B. Pan, Y.G. Zhou, L. He, J. Sun, Dependence of ductility on free volume in a CuZr-based metallic glass, *Adv. Eng. Mater.* 11 (2009) 177–181.
- [60] F. Jiang, Y.L. Zhao, L.C. Zhang, S.B. Pan, Y.G. Zhou, L. He, J. Sun, The coupling effect of small nanocrystals and free volume on the ductility of $\text{Cu}_{46}\text{Zr}_{47}\text{Al}_7$ bulk metallic glass alloy, *Adv. Eng. Mater.* 11 (2009) 374–379.
- [61] Y. Fan, T. Washita, T. Egami, How thermally activated deformation starts in metallic glass, *Nat. Commun.* 5 (2014) 5083.
- [62] C.H. Rycroft, E. Bouchbinder, Fracture toughness of metallic glasses: annealing-induced embrittlement, *Phys. Rev. Lett.* 109 (2012), 194301.
- [63] M. Fan, M.L. Wang, K. Zhang, Y.H. Liu, C.S. O'Hern, Effects of cooling rate on particle rearrangement statistics: rapidly cooled glasses are more ductile and less reversible, *Phys. Rev. E* 95 (2017), 022611.
- [64] E. Teatum, J.K. Gschneidner, J. Waber, *Compilation of Calculated Data Useful in Predicting Metallurgical Behavior of the Elements in Binary Alloy Systems*, LA-2345, Los Alamos Scientific Laboratory, University of California, Los Alamos, NM, USA, 1960.
- [65] T. Egami, S.J.L. Billinge, in: R.W. Cahn (Ed.), *Underneath the Bragg Peaks*, Pergamon Materials Series Vol. 7, Elsevier, Oxford, 2003.
- [66] H.X. Li, C.Q. Li, D. Cao, W.M. Yang, Q. Li, Z.P. Lu, Influences of oxygen on plastic deformation of a Fe-based bulk metallic glass, *Scripta Mater* 135 (2017) 24–28.
- [67] A.L. Greer, Y.Q. Cheng, E. Ma, Shear bands in metallic glasses, *Mater. Sci. Eng. R* 74 (2013) 71–132.
- [68] Ketkaew, W. Chen, H. Wang, A. Datye, M. Fan, G. Pereira, U.D. Schwarz, Z. Liu, R. Yamada, W. Dmowski, M.D. Shattuck, C.S. O'Hern, T. Egami, E. Bouchbinder, J. Schroers, Mechanical glass transition revealed by the fracture toughness of metallic glasses, *Nat. Commun.* 9 (2018) 3271.
- [69] M. Vasoya, C.H. Rycroft, E. Bouchbinder, Notch fracture toughness of glasses: dependence on rate, age, and geometry, *Phys. Rev. Applied* 6 (2016), 024008.
- [70] L. Yang, G.Q. Guo, L.Y. Chen, C.L. Huang, T. Ge, D. Chen, P.K. Liaw, K. Saksli, Y. Ren, Q.S. Zeng, B. LaQua, F.G. Chen, J.Z. Jiang, Atomic-scale mechanisms of the glass-forming ability in metallic glasses, *Phys. Rev. Lett.* 109 (2012) 195503.
- [71] G.Q. Guo, L. Yang, Structural mechanisms of the microalloying-induced high glass-forming abilities in metallic glasses, *Intermetallics* 65 (2015) 66–74.
- [72] Q. Wang, C.T. Liu, Y. Yang, J.B. Liu, Y.D. Dong, J. Lu, The atomic-scale mechanism for the enhanced glass-forming-ability of a Cu-Zr based bulk metallic glass with minor element additions, *Sci. Rep.* 4 (2014) 4648.
- [73] L. Zhang, Y.Q. Cheng, A.J. Cao, J. Xu, E. Ma, Bulk metallic glasses with large plasticity: composition design from the structural perspective, *Acta Mater.* 57 (2009) 1154–1164.
- [74] Y.Q. Cheng, E. Ma, Atomic-level structure and structure-property relationship in metallic glasses, *Prog. Mater. Sci.* 56 (2011) 379–473.